Hindawi
Advances in Civil Engineering
Volume 2019, Article ID 5678427, 10 pages
https://doi.org/10.1155/2019/5678427

Research Article

Research on Failure Mechanism and Parameter Sensitivity of Zonal Disintegration in Deep Tunnel

Xutao Zhang[1,2] **Qiang Gao**[3] **Shicai Cui**[2] **and Changrui Duan**[1]

[1]*State Key Laboratory of Deep Coal Mining and Environment Protection, Huainan 232000, China*
[2]*School of Architecture and Engineering, Liaocheng University, Liaocheng 252059, China*
[3]*Geotechnical and Structural Engineering Research Center, Shandong University, Jinan, Shandong 250061, China*

Correspondence should be addressed to Xutao Zhang; zhangxutao@lcu.edu.cn and Qiang Gao; gaoqiangsdu@163.com

Received 30 September 2018; Revised 27 November 2018; Accepted 11 December 2018; Published 3 January 2019

Academic Editor: Lei Wang

With the increase of excavation depth, the zonal disintegration phenomenon appears in the deep rock mass, which is quite different from the failure mode of shallow tunnel. In order to analyse the failure mechanism of this phenomenon, an elastoplastic softening damage model was put forward based on the softening damage characteristics of deep rock mass. The constitutive equations, the equilibrium equations, and the failure criterion were deduced. The theoretical solutions of radial displacement and radial stresses and tangential stresses of deep surrounding rock mass were calculated. The distribution law of zonal disintegration in deep tunnel was obtained. The theoretical solutions presented an oscillating mode. The theoretical calculated widths of fracture zones were in good agreement with the in situ test data. Besides, the sensitivity of different parameters to fracture morphology was calculated and analysed. The results show that the relative loading strength has a controlling role in the zonal disintegration morphology, followed by the cohesion force and deformation modulus, and the internal friction angle is the least. This study reveals the morphological characteristics and influencing factors of zonal disintegration, which provides a basis for the prediction and support control of fracture modes.

1. Introduction

With the increasing demand for deep underground space utilization and various resource developments, significant nonlinear deformation and failure occurs in the surrounding rock of the tunnel. Many zonal disintegration phenomena [1–3] were found during the monitoring of deep rock mass engineering (Figure 1), and many experts and scholars have studied this phenomenon.

Different test methods were used to study the mechanism of zonal disintegration: the cement mortar was used as the model test material, and the zonal disintegration phenomenon was observed [4] (Figure 2). The failure characteristics of the zonal disintegration in the deep surrounding rock were analysed by the geomechanical model tests [5]. Many experts have studied the fragmentation phenomenon by numerical simulation [6, 7]. At present, many theories about the rupture of surrounding rock have been proposed: the occurrence of rupture of surrounding rock is related to the magnitude of the geostress and the strength of the rock [8]; the surrounding rock of the deep roadway will be subject to zonal rupture under the influence of continuous tensile and brittle fracture [9–11].

The current research studies mainly focus on the formation mechanism of zonal disintegration, and less attention is paid to fracture morphology caused by intrinsic factors of surrounding rock. The fracture morphology contains the number and the depth of the fracture zones and will affect the stability of the surrounding rock. So, the sensitivity of intrinsic factors determined to the zonal disintegration morphology should be sorted, and then its influence on the stability of surrounding rock can be analysed.

An elastoplastic model and failure criterion was put forward based on the damage property of rock mass. The morphology of zonal disintegration was obtained through theoretical calculation. Then, the sensitivity of different parameters to the fracture morphology was analysed. This study reveals the morphological characteristics and influencing factors of zonal disintegration, which provides a basis for the prediction and support control of fracture modes.

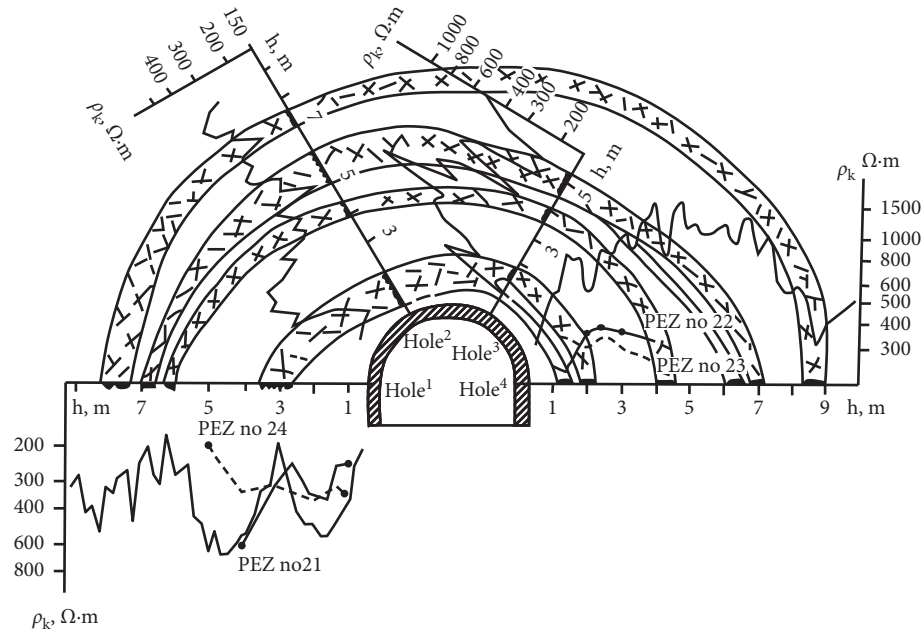

Figure 1: Talmyrskii Mine in depth of 1050 m.

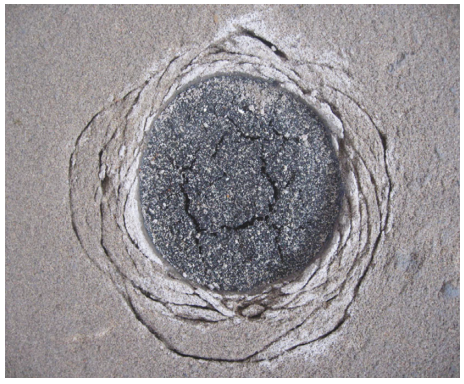

Figure 2: Zonal disintegration phenomena obtained by model test.

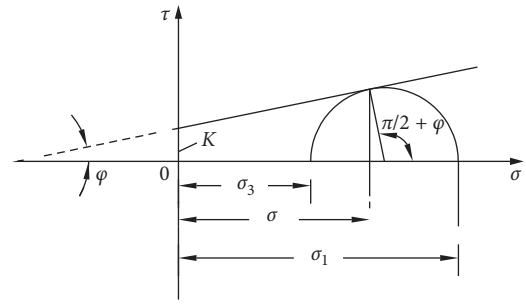

Figure 3: Envelop of Mohr circles of principle stresses.

2. The Calculation of Elastoplastic Displacement Field and Stress Field in Deep Rock Mass

2.1. Elastoplastic Softening Damage Model. For rock masses, the usual yield criterion is the Mohr–Coulomb yield criterion (Figure 3). According to the yield criterion, the shear strength of the rock mass τ depends on the normal stress σ on the shear slip plane and the shear strength can be expressed as

$$\tau = \sigma \tan \varphi + c, \tag{1}$$

where c is cohesive force, φ is internal friction angle.

According to classical elastic theory,

$$\begin{cases} \sigma = \dfrac{\sigma_1 + \sigma_3}{2} - \dfrac{\sigma_1 - \sigma_3}{2} \sin \varphi, \\ \tau = \dfrac{\sigma_1 - \sigma_3}{2} \cos \varphi. \end{cases} \tag{2}$$

After substituting equation (2) into the yield criterion formula and the yield criterion formula can be written as

$$\sigma_1 - A\sigma_3 = \sigma_c, \tag{3}$$

where $A = (1 + \sin \varphi)/(1 - \sin \varphi)$, $\sigma_c = 2c \cos \varphi/(1 - \sin \varphi)$, and the physical meaning of σ_c is the uniaxial compressive strength of rock.

The surrounding rock under high geostress conditions exhibits certain ductility. After exceeding the peak strength, the rock masses are presented the strain softening characteristics [12], as shown in Figure 4.

Figure 4 shows the stress-strain curves of deep rock masses under high stress conditions, where σ_f is peak stress, ε_f is peak strain, and ε_u is ultimate strain. According to the postpeak strain softening mechanical properties of rock under deep high geostress conditions, the stress-strain relationship is simplified (Figure 5) [13].

In Figure 5, the OA segment is simplified as a linear elastic zone, in which E is the elastic modulus; the AC segment is the plastic bearing zone [14], in which the AB segment is the prepeak plastic hardening segment, in which E_0 is the deformation modulus; and the BC segment is the postpeak plastic damage softening segment, in which $|M|$ is the softening modulus, ε_1' is the deformation in the direction of the principal stress of the postpeak

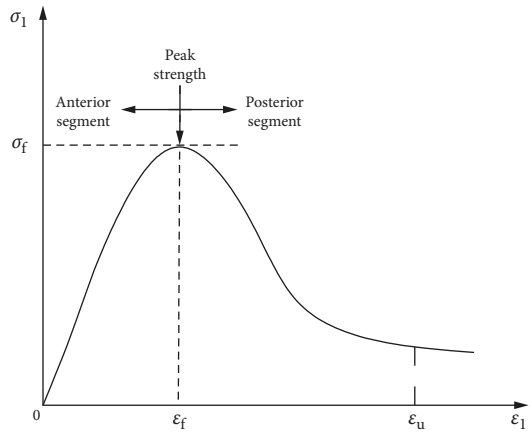

Figure 4: Relation curve of differential stress and axial strain of rock in deep.

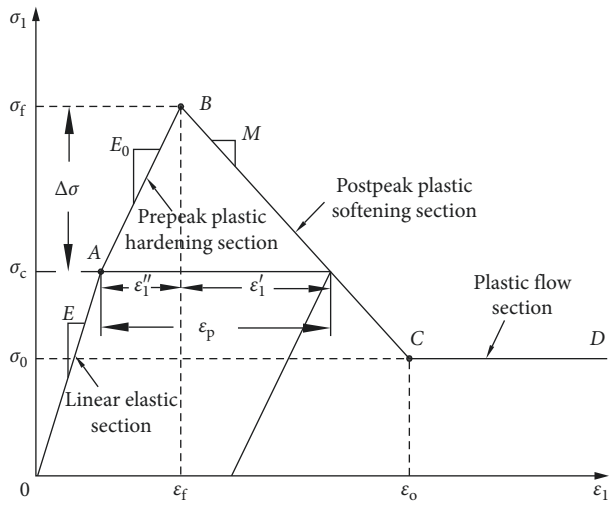

Figure 5: Stress-strain curve with softening.

plastic softening section, and ε_1'' is the irreversible deformation produced by the prepeak plastic hardening section; the CD section is the plastic flow area and σ_0 is the residual stress strength.

The total irreversible deformation throughout the plastic deformation process is written as

$$\varepsilon_1^{\mathrm{p}} = \varepsilon_1' + \varepsilon_1''. \tag{4}$$

The microcracks begin to propagate near the yield point, and the volumetric strain of rock increases as well (Figure 6). Therefore, the damage threshold of rock is at the yield point [15]. d is introduced to describe the surrounding rock damage, and the mechanic characteristics of damaged rock under the high geostress are described with the following damage evolution law [16]:

$$d = d(\varepsilon_1) = \begin{cases} 0, & \varepsilon_1 < \varepsilon_f, \\ \dfrac{\varepsilon_u}{\varepsilon_1}\dfrac{\varepsilon_1 - \varepsilon_f}{\varepsilon_u - \varepsilon_f}, & \varepsilon_f \le \varepsilon_1 < \varepsilon_u, \\ 1, & \varepsilon_1 \ge \varepsilon_u. \end{cases} \tag{5}$$

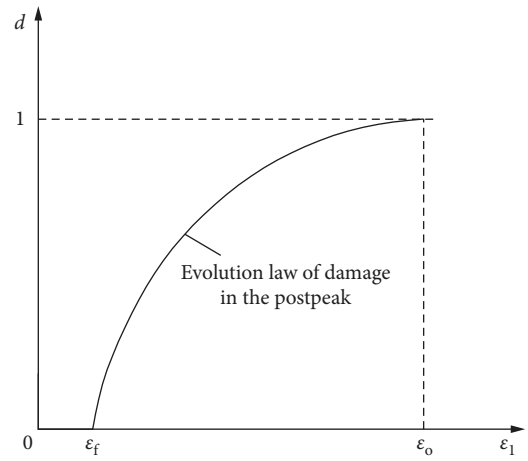

Figure 6: Damage strain curve.

The evolution law hypothesizes that there is no damage at the elastic segment, and the rock masses enter damage state when yielding to plasticity.

The relationship between the principal stresses in the plastic softening section is

$$\sigma_1 - A\sigma_3 = \sigma_c - \frac{|M|\varepsilon_1'}{(1-d)} = \sigma_c - \frac{|M|\varepsilon_1''}{((1-d)\xi)} = \sigma_c + \frac{|M|\varepsilon_3'}{((1-d)\beta)}, \tag{6}$$

where β is postpeak Poisson ratio, $\beta = -\varepsilon_3'/\varepsilon_1'$; ξ is modulus parameters, and $\xi = |M/E_0|$.

So, the irreversible deformation can be expressed as

$$\begin{cases} \varepsilon_1^{\mathrm{p}} = \varepsilon_1' + \varepsilon_1'' = \varepsilon_1'(1+\xi) = \dfrac{(\sigma_c - \sigma_1 + A\sigma_3)(1-d)(1+\xi)}{|M|}, \\ \varepsilon_3^{\mathrm{p}} = \varepsilon_3' + \varepsilon_3'' = -\varepsilon_1'(\beta + \upsilon\xi) = -\dfrac{(\sigma_c - \sigma_1 + A\sigma_3)(1-d)(\beta+\upsilon\xi)}{|M|}. \end{cases} \tag{7}$$

The strain at the elastic section is

$$\begin{cases} \varepsilon_1^{\mathrm{e}} = \dfrac{1-\upsilon^2}{E}\left(\sigma_1 - \dfrac{\upsilon}{1-\upsilon}\sigma_3\right), \\ \varepsilon_3^{\mathrm{e}} = \dfrac{1-\upsilon^2}{E}\left(\sigma_3 - \dfrac{\upsilon}{1-\upsilon}\sigma_1\right). \end{cases} \tag{8}$$

The total strain is written as

$$\begin{cases} \varepsilon_1 = \varepsilon_1^{\mathrm{e}} + \varepsilon_1^{\mathrm{p}} = \left(\dfrac{1-\upsilon^2}{E} - \dfrac{(1+\xi)}{|M|}\right)\sigma_1 \\ \qquad + \left(\dfrac{-(1+\upsilon)\upsilon}{E} + \dfrac{(1-d)(1+\xi)A}{|M|}\right)\sigma_3 + \dfrac{(1-d)(1+\xi)\sigma_c}{|M|}, \\ \varepsilon_3 = \varepsilon_3^{\mathrm{e}} + \varepsilon_3^{\mathrm{p}} = \left(\dfrac{-(1+\upsilon)\upsilon}{E} + \dfrac{(1-d)(\beta+\xi\upsilon)}{|M|}\right)\sigma_1 \\ \qquad + \left(\dfrac{1-\upsilon^2}{E} - \dfrac{(1-d)(\beta+\xi\upsilon)A}{|M|}\right)\sigma_3 + \dfrac{-(1-d)(\beta+\xi\upsilon)\sigma_c}{|M|}. \end{cases} \tag{9}$$

The plastic constitutive formula can be expressed as follows:

$$\begin{cases} \sigma_1 = k_1\varepsilon_1 + m_1\varepsilon_3 + n_1, \\ \sigma_3 = k_2\varepsilon_1 + m_2\varepsilon_3 + n_2, \end{cases} \tag{10}$$

where

$$\begin{aligned} k_1 &= \frac{b_2}{a_1b_2 - a_2b_1}, \\ m_1 &= \frac{-b_1}{a_1b_2 - a_2b_1}, \\ n_1 &= \frac{b_1c_2 - b_2c_1}{a_1b_2 - a_2b_1}, \\ k_2 &= \frac{-a_2}{a_1b_2 - a_2b_1}, \\ m_2 &= \frac{a_1}{a_1b_2 - a_2b_1}, \\ n_2 &= \frac{a_2c_1 - a_1c_2}{a_1b_2 - a_2b_1}, \\ a_1 &= \frac{1-v^2}{E} - \frac{(1-d)(1+\xi)}{|M|}, \\ b_1 &= \frac{-(1+v)v}{E} + \frac{(1-d)(1+\xi)A}{|M|}, \\ c_1 &= \frac{(1-d)(1+\xi)\sigma_c}{|M|}, \\ a_2 &= \frac{-(1+v)v}{E} + \frac{(1-d)(\beta+\xi v)}{|M|}, \\ b_2 &= \frac{1-v^2}{E} - \frac{(1-d)(\beta+\xi v)A}{|M|}, \\ c_2 &= \frac{-(1-d)(\beta+\xi v)\sigma_c}{|M|}. \end{aligned} \tag{11}$$

2.2. Elastoplastic Stress Field of Surrounding Rock in Circular Tunnel. Taking the deep circular horizontal tunnel as an example, the stress state of the rocks around the tunnel is analysed. The surrounding rock in the deep tunnel is abstracted as a thick-walled cylinder model. The pressure on the outer wall of the cylinder is P_0 , the radius is b, the excavation radius of the tunnel is a, and the radius of the plastic bearing zone in the surrounding rock is r_{12} (Figure 7).

Due to the axial symmetry of the thick-walled cylinder model, it is more convenient to analyse it in the polar coordinate system (r, θ), and the displacement at any position in the surrounding rock is represented by u. Further analysis shows that there are two nonzero items ε_r and ε_θ in the strain tensor ε_{ij}, so the simplified geometric equation is written as

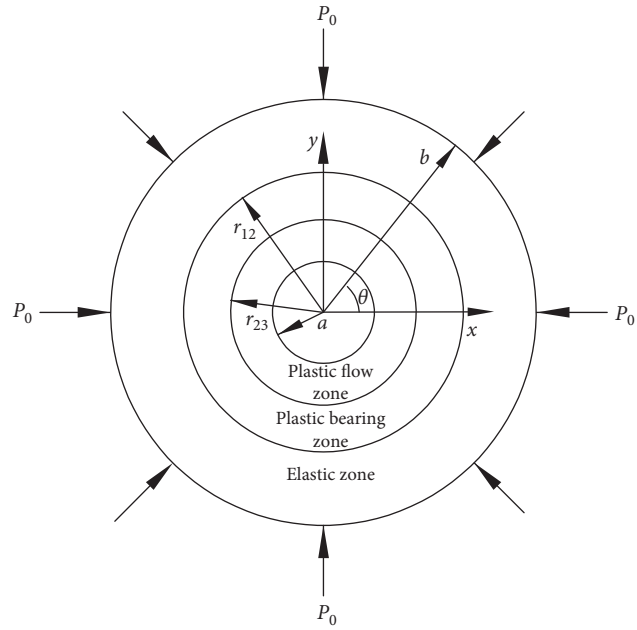

Figure 7: Forces on circular tunnel.

$$\begin{aligned} \varepsilon_r &= \frac{du}{dr}, \\ \varepsilon_\theta &= \frac{u}{r}. \end{aligned} \tag{12}$$

The constitutive equations (8) and (10) are expressed in cylindrical coordinates as follows:

(i) The elastic zone

$$\begin{cases} \sigma_{\theta e} = (\lambda + 2G)\dfrac{u}{r} + \lambda\dfrac{du}{dr}, \\ \sigma_{re} = \lambda\dfrac{u}{r} + (\lambda + 2G)\dfrac{du}{dr}. \end{cases} \tag{13}$$

(ii) The plastic bearing zone

$$\begin{cases} \sigma_{\theta p} = k_1\dfrac{u}{r} + m_1\dfrac{du}{dr} + n_1, \\ \sigma_{rp} = k_2\dfrac{u}{r} + m_2\dfrac{du}{dr} + n_2. \end{cases} \tag{14}$$

(1) Stress solution in plastic bearing zone

Assuming that physical strength is neglected, the equivalent equation is written as

$$\frac{\partial\sigma_{rp}}{\partial r} + \frac{\sigma_{rp} - \sigma_{\theta p}}{r} = 0. \tag{15}$$

After substituting equation (14) into equation (15), the equivalent equation can be expressed as follows:

$$\frac{d^2u_p}{dr^2}+\frac{B_p}{r}\frac{du_p}{dr}+\frac{C_p}{r^2}u_p=\frac{D_p}{r}, \tag{16}$$

where $B_p=((k_2+m_2-m_1)/m_2)$, $C_p=-(k_1/m_2)$, $D_p=((n_1-n_2)/m_2)$.

Plastic zone displacement u_p can be calculated as

$$u_p=r^{-W}\left[\frac{D_p}{\left(B_p-W_p\right)\left(W_p+1\right)}r^{W_p+1}+\frac{C_{1p}}{2W_p-B_p+1}r^{2W_p-B_p+1}+C_{2p}\right]=\frac{D_p}{B_p+C_p}r+\frac{C_{1p}}{2W_p-B_p+1}r^{W_p-B_p+1}+C_{2p}r^{-W_p}, \tag{17}$$

where $W_p=(B_p-1+\sqrt{(B_p-1)^2-4C_p}/2)$, C_{1p} and C_{2p} is undetermined coefficients.

After substituting equation (17) into the plastic constitutive equation, the stresses can be expressed as follows:

$$\begin{cases}\sigma_{\theta p}=J_{1p}C_{1p}r^{W_p-B_p}+K_{1p}C_{2p}r^{-W_p-1}+L_{1p},\\ \sigma_{rp}=J_{2p}C_{1p}r^{W_p-B_p}+K_{2p}C_{2p}r^{-W_p-1}+L_{2p},\end{cases} \tag{18}$$

where

$$\begin{aligned}J_{1p}&=\frac{\left(k_1+m_1W_p-m_1B_p+m_1\right)}{2W_p-B_p+1},\\ K_{1p}&=k_1+m_1,\\ L_{1p}&=\frac{k_1+m_1}{B_p+C_p}D_p+n_1,\\ J_{2p}&=\frac{\left(k_2+m_2W_p-m_2B_p+m_2\right)}{2W_p-B_p+1},\\ K_{2p}&=k_2+m_2,\\ L_{2p}&=\frac{k_2+m_2}{B_p+C_p}D_p+n_2.\end{aligned} \tag{19}$$

The inner boundary ($r=a$) of the plastic bearing zone satisfies the following boundary conditions:

$$\sigma_{rp}\big|_{r=a}=0. \tag{20}$$

(2) Stress solution in elastic zone

The equilibrium equation for the elastic zone can also be expressed as

$$\frac{\partial\sigma_{re}}{\partial r}+\frac{\sigma_{re}-\sigma_{\theta e}}{r}=0. \tag{21}$$

After substituting equation (13) into equation (21), the equivalent equation can be expressed as follows:

$$\frac{d^2u_e}{dr^2}+\frac{1}{r}\frac{du_e}{dr}-\frac{1}{r^2}u_e=0. \tag{22}$$

Elastic zone displacement u_e can be calculated as

$$u_e=C_{1e}r+C_{2e}r^{-1}, \tag{23}$$

where C_{1e} and C_{2e} are undetermined coefficients.

After substituting equation (23) into the elastic constitutive equation, the stresses can be expressed as follows:

$$\begin{cases}\sigma_{\theta e}=2(\lambda+G)C_{1e}+2GC_{2e}r^{-2},\\ \sigma_{re}=2(\lambda+G)C_{1e}-2GC_{2e}r^{-2}.\end{cases} \tag{24}$$

The outer boundary ($r=b$) of the plastic bearing zone satisfies the following boundary conditions:

$$\sigma_{re}\big|_{r=b}=P_0. \tag{25}$$

At the elastoplastic boundary ($r=r_{12}$), the stresses satisfied the yield criterion shown in equation (3), so the following boundary conditions are satisfied as

$$\begin{cases}\sigma_\theta-A\sigma_r\big|_{r=r_{12}}=\sigma_c,\\ \sigma_{re}\big|_{r=r_{12}}=\sigma_{rp}\big|_{r=r_{12}},\\ \sigma_{\theta e}\big|_{r=r_{12}}=\sigma_{\theta p}\big|_{r=r_{12}}.\end{cases} \tag{26}$$

After substituting the boundary conditions (20), (25), and (26) into equations (18) and (24), respectively, the values of the determined parameters C_{1p}, C_{2p}, C_{1e}, C_{2e} and the range of the plastic loading zone r_{12} can be calculated, and then the elastoplastic stress field of entire circular tunnel can be calculated.

2.3. Determination of Fracture Zones and Nonfracture Zones. As shown in Figure 8, the tangential strain $\varepsilon_\theta=0$ and the stress $\sigma_\theta=\sigma_r$ in the elastic region away from the tunnel. In the plastic zone near the tunnel, the stresses satisfied equation (26) at the boundary between the plastic bearing zone and elastic zone. The strength of the rock mass is determined by the bite force, bonding force, and friction of the rock mass.

In the plastic bearing zone, with the increase of deformation, the unevenness on the sliding surface is flattened, and the bite force gradually decreases, so the strength of the rock body gradually decreases to residual strength σ_0 at the boundary $r=r_{23}$ of the plastic flow zone. The residual strength is determined by the bond strength and friction of the rock mass. At this boundary, the stress condition is satisfied as follows:

$$\sigma_\theta-A\sigma_r=\sigma_0. \tag{27}$$

When the elastoplastic stress field of the surrounding rock in the deep circular tunnel is obtained, the boundary conditions equation (27) can be used to determine the fracture zone and nonfracture zone of the deep rock mass. Assuming that the stresses of the deep rock mass in the plastic bearing zone satisfied equation (27), the rock mass enters the plastic flow zone and ruptured phenomenon occurs, resulting in the first fracture zone with a concomitant decrease in tangential stress and radial stress. The radial

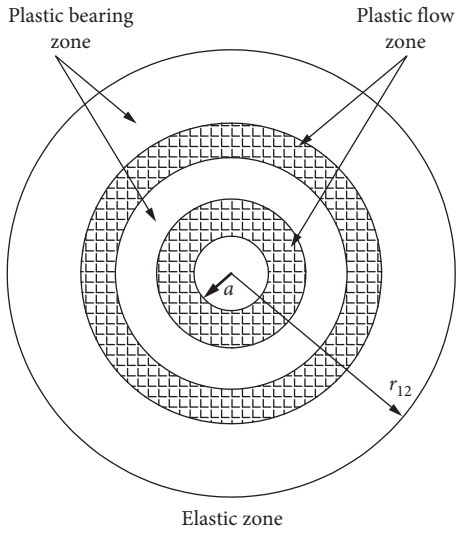

Figure 8: Zonal disintegration of surrounding rock of tunnel after excavation.

displacement also increases. The stresses wave continues to propagate to the interior. When the redistribution stresses of the surrounding rock satisfied equation (27) again, the stresses are further released and a second fracture zone is obtained. This cycle continues until the redistribution stresses condition cannot meet the boundary. The fracture zone created by each stresses' release is generally a certain distance away from the new excavation boundary, and this zone forms a nonfracture zone. As the location of the fracture zone is far from the inner boundary of the tunnel, the stress field is gradually reduced, the destruction of the surrounding rock is gradually stopped, and the rock body gradually stabilizes, and thus, the phenomenon that the fracture zones and the nonfracture zones appear alternately, shown in Figure 7.

In the range of the plastic bearing zone, substituting equation (18) into equation (12), an expression for the radius r_{23} of the plastic flow zone is obtained:

$$\left(J_{1p} - AJ_{2p}\right)C_{1p}r_{23}^{W_p - B_p} + \left(K_{1p} - AK_{2p}\right)C_{2p}r_{23}^{-W_p - 1} + L_{1p} - AL_{2p} - \sigma_0 = 0. \tag{28}$$

Through the above solution, the radius r_{23} of the plastic flow zone can be obtained, and then the distribution of the surrounding rock zonal disintegration in the circular tunnel can be obtained.

3. Zonal Disintegration Example

3.1. Selection of Calculation Parameters. Taking the surrounding rock of tunnel with a near-kilometer level in Huainan Dingji Coal Mine as a zonal disintegration example, the equivalent radius of the tunnel is $a = 2.5$ m, the radius of the calculated area is $b = 20$ m, the geostress is $P_0 = 34$ MPa, the rock density is $\rho = 2.70$ g/cm^3, the elastic modulus is $E = 77.82$ GPa, the deformation modulus is $E_0 = 12.97$ GPa, cohesion $c = 9$ MPa , and the internal friction angle is $\varphi = 32^\circ$.

3.2. Calculation Result Analysis. Using the above calculation parameters, the radius of the plastic zone of the surrounding rock is calculated as $\rho = 12.63$ m; that is, the surrounding rock is in the plastic state within the range of $2.5\ \text{m} \le \rho \le 12.63$ m, and the surrounding rock is in the elastic state within the range of $12.63\ \text{m} < \rho \le 20$ m. Figure 8 is a calculated solution of radial displacement u, radial stress σ_r, and tangential stress σ_θ of tunnel surrounding rock.

Figure 9 shows that the radial displacement, radial stress, and tangential stress around the tunnel exhibit an oscillation attenuation law in which peaks and troughs appear alternately, and the amplitude of the oscillation decreases gradually with the distance from the tunnel wall.

The theoretical value of the fracture zone was calculated by equation (27), as shown in Table 1. Table 1 shows that the number of fracture zone is four and the fracture zone depth is 11.36 m. The radius of each fracture zone is in good agreement with the in situ measured values [17], confirming the applicability of this calculation model to analyse the zonal disintegration phenomenon. With the help of borehole television, the zonal disintegration is observed which is alternation phenomenon of the fracture zone and nonfracture zone in reference [17]. At the same time, the range and radius of the fracture zone were also measured.

From Figure 9 and Table 1, it can be seen that the stresses of the surrounding rock in the nonfracture zone are in the peak area, the stress value is relatively large, the displacement is in the trough area, and the displacement value is relatively small; otherwise, the stresses of the surrounding rock in the fracture zone are in the trough area, and the stress value is relatively small, the displacement is in the peak area, and the displacement value is relatively large, which is consistent with the actual situation.

4. Analysis of Sensitivity Parameters of Zonal Disintegration Morphology

Zonal disintegration, a special form of deep rock damage, may cause large-scale disaster. Current research studies are focused on exploring its formation mechanism but ignore to explore the production conditions and failure patterns of zonal disintegration and its related influencing factors. The problem is the basic mechanism to predict disintegrative range and take preventive measures such as grouting, anchoring, and so on. The analysis of sensitivity parameters of zonal disintegration morphology has important implications to reveal failure patterns of zonal disintegration and its influencing factors and to build prediction, prevention, and control measures for different evolution mode of zonal disintegration.

4.1. Sensitivity Analysis. Sensitivity analysis is a method for analysing system stability and has been applied in geotechnical engineering [18]. With a system, its system characteristics P are mainly determined by several parameters $a = (a_1, a_2, \ldots, a_n)$. In a certain reference parameter $a^* = (a_1^*, a_2^*, \ldots, a_n^*)$, the reference characteristic is P^*. The trend of the system characteristics P deviating from the state

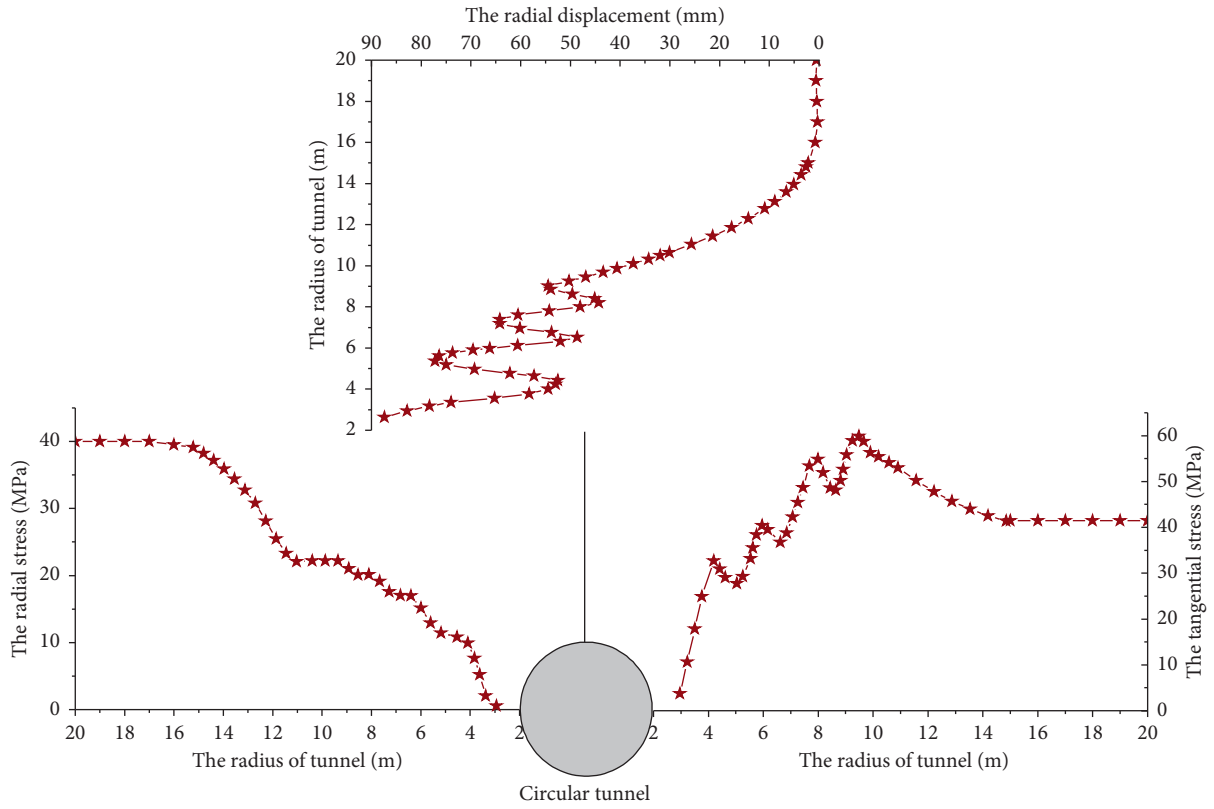

Figure 9: Calculated solutions of displacement and stress of surrounding rock in tunnel.

Table 1: Comparison between theoretical calculation result and in situ test value.

	Fracture zone	In situ test value	Theoretical calculation result
1	Inner radius (m)	2.50	2.50
	External radius (m)	4.99	4.64
2	Inner radius (m)	5.75	5.52
	External radius (m)	6.55	6.75
3	Inner radius (m)	7.74	7.56
	External radius (m)	8.78	8.93
4	Inner radius (m)	9.87	9.65
	External radius (m)	10.40	11.36

of the reference characteristic P^* is analysed due to the changes in these parameters within their respective possible ranges. This analysis method is called sensitivity analysis.

Firstly, a system model should be established, which is a functional relationship between system characteristics and parameters $P = f(a_1, a_2, \ldots, a_n)$. This kind of functional relationship, if possible, is expressed analytically, for more complex systems; it can also be represented by calculated methods (such as finite element models, etc.) or graphs. Establishing a system model that is close to the actual system is a crucial task for effectively performing parameter sensitivity analysis.

After setting up the system model, a reference parameter set must be given based on the specific issues to be discussed. For example, in order to analyse the susceptibility of the stability of an underground project to changes in its rock mechanics parameters, the recommended values of the rock mechanics parameters for the project site may be taken as the reference parameter set. After the reference parameter set is determined, sensitivity analysis can be performed on each parameter. When analysing the influence of parameter a_k on the characteristics P, the rest of the parameters can be taken as the reference value and fixed, and within the range of possible changes, the system characteristics are expressed as

$$P = f(a_1^*, \ldots, a_{k-1}^*, a_k, a_{k+1}^*, \ldots, a_n^*). \tag{29}$$

If small changes in a_k cause large changes in P, a_k is a highly sensitive parameter; however, if large changes in a_k cause slight changes in P, a_k is a low sensitive parameter.

To compare the sensitivities of different parameters, the sensitivity factor is defined as

$$S(a_k) = \max\left\{\left(\frac{U_{a_k \max} - U^*}{U^*}\right), \left(\frac{U^* - U_{a_k \min}}{U^*}\right)\right\}, \tag{30}$$

where $S(a_k)$ is the sensitivity of the parameter a_k; U^* is the reference characteristic value corresponding to the reference parameters set; and $U_{a_k \max}$ and $U_{a_k \min}$ are the maximum and minimum characteristic values within the variation range of the f parameter a_k, respectively.

4.2. Reference Parameters. In order to analyse the sensitivity effects of various parameters on the number of fracture

zones and the depth of fracture zones, the mechanical parameters of tunnel surrounding rock in Dingji Coal Mine are used as reference parameter values. The values are as follows: deformation modulus E_0 = 12.97 GPa, cohesion c = 9 MPa, internal friction angle $\varphi = 32^\circ$, and relative loading strength $\kappa = P_z/\sigma_c = 2$, where κ is the ratio of tunnel axial stress to compressive strength of surrounding rock which is a parameter can reflect the geostress state. The parameters change ranges are selected according to the parameter distribution rules indicated by the test results and shown in Table 2.

4.3. The Impact of Various Parameters on the Fracture Zone. Based on the above-mentioned ranges of basic parameters and theoretical calculation, the effect of each parameter on the number and depth of the fracture zones in the surrounding rock are obtained (Figure 10).

With the increase of surrounding rock mechanical parameters (deformation modulus, cohesion, and internal friction angle), the depth of the fracture zone decreases approximately linearly, and the number of fracture zones is also trapezoidally decreased with the increase of mechanical parameters.

With the increase of the relative loading strength, the depth of the fracture zone firstly increases gently, and when the relative loading strength continues to increase, the trend of the increase in the depth of the fracture zone became acute, and it increases steadily in the later period. It shows that there is a critical value and when the relative loading strength is higher than this value, the depth of the fracture zone will increase rapidly. It can also be seen from the number of fracture zone that when the relative loading strength is small, only one layer fracture zone occurs in the wall of the tunnel; when the relative loading strength is greater than a certain amount, the zonal disintegration phenomenon occurs.

4.4. Comparison of Sensitivity of Each Parameter. In order to further explain the influence of various parameters on the morphology of zonal disintegration, the sensitivity analysis histogram is made according to the sensitivity definition given in equation (30) and each parameter within the change range (Figure 11).

Figure 11 shows that the sensitivity of parameters affecting the number and depth of fracture zone is in the order relative loading strength > cohesion force > internal friction angle > deformation modulus. The sensitivity of the relative loading strength is the largest, which shows that the strength of the surrounding rock itself and the state of the geostress are the most sensitive to the zonal disintegration of the tunnel.

Relevant theoretical research studies [19] and the similar model tests [4, 5] about zonal disintegration indicate that the relative loading strength is an important condition for the zonal disintegration in the deep rock mass. The relative loading strength sensitivity is significantly higher than the other four factors in Figure 10, indicating that the relative loading strength is the primary condition to determine whether the zonal disintegration occurs. From the calculation results in Figure 9, it can also be seen that only when the relative loading strength is greater than a certain amount, the surrounding rock will have a zonal fracture phenomenon.

Table 2: Basic values and variations of parameters.

Parameter name	E_0 (GPa)	c (MPa)	φ (°)	κ
Basic values	12.97	9	43	2
Variation range	6–20	5–15	35–50	0.5–3

During the excavation process of deep tunnels, different excavation methods lead to different unloading times during the adjustment and redistribution of geostress. The sensitivity of the unloading times is second only to the relative loading strength in the formation process and destruction law of zonal disintegration; unloading time plays an important role in surrounding rock of deep tunnel.

The cohesion force, deformation modulus, and internal friction angle of the rock mass are the basic mechanical parameters of the rock mass, and the sensitivity of the internal friction angle is the lowest. Therefore, the accuracy of the cohesion force and deformation modulus must be taken seriously under the evaluation of the surrounding rock mechanics parameters.

5. Conclusion

(1) Based on the softening damage characteristics of deep rock masses, the displacement and stress distributions of tunnel surrounding rock are calculated using the elastoplastic softening damage model. The radial displacement, radial stress, and tangential stress of the surrounding rock alternately oscillate between peaks and troughs. According to the law of change, the width and number of fracture zones in the theoretical calculations are in good agreement with the in situ measured values, confirming the applicability of the model in analysing the zonal disintegration phenomenon. For deep rock mass under high geostress conditions, due to the oscillation-type changing rules of radial displacement and stress field in the surrounding rock of deep tunnel, the fracture zone and the nonfracture zone alternately appear, resulting in the occurrence of zonal disintegration.

(2) The parameter sensitivity affecting the zonal disintegration morphology of surrounding rock in deep tunnel is in the order relative loading strength > cohesion force > internal friction angle > deformation modulus. The relative loading strength is the decisive condition for the zonal disintegration phenomenon. The ranking of the relevant mechanical parameters is of great significance for the prediction, prevention, and remediation measures of different zonal disintegration evolution patterns.

(3) This theoretical calculation method has a broader application prospect. Then, it also indicates the

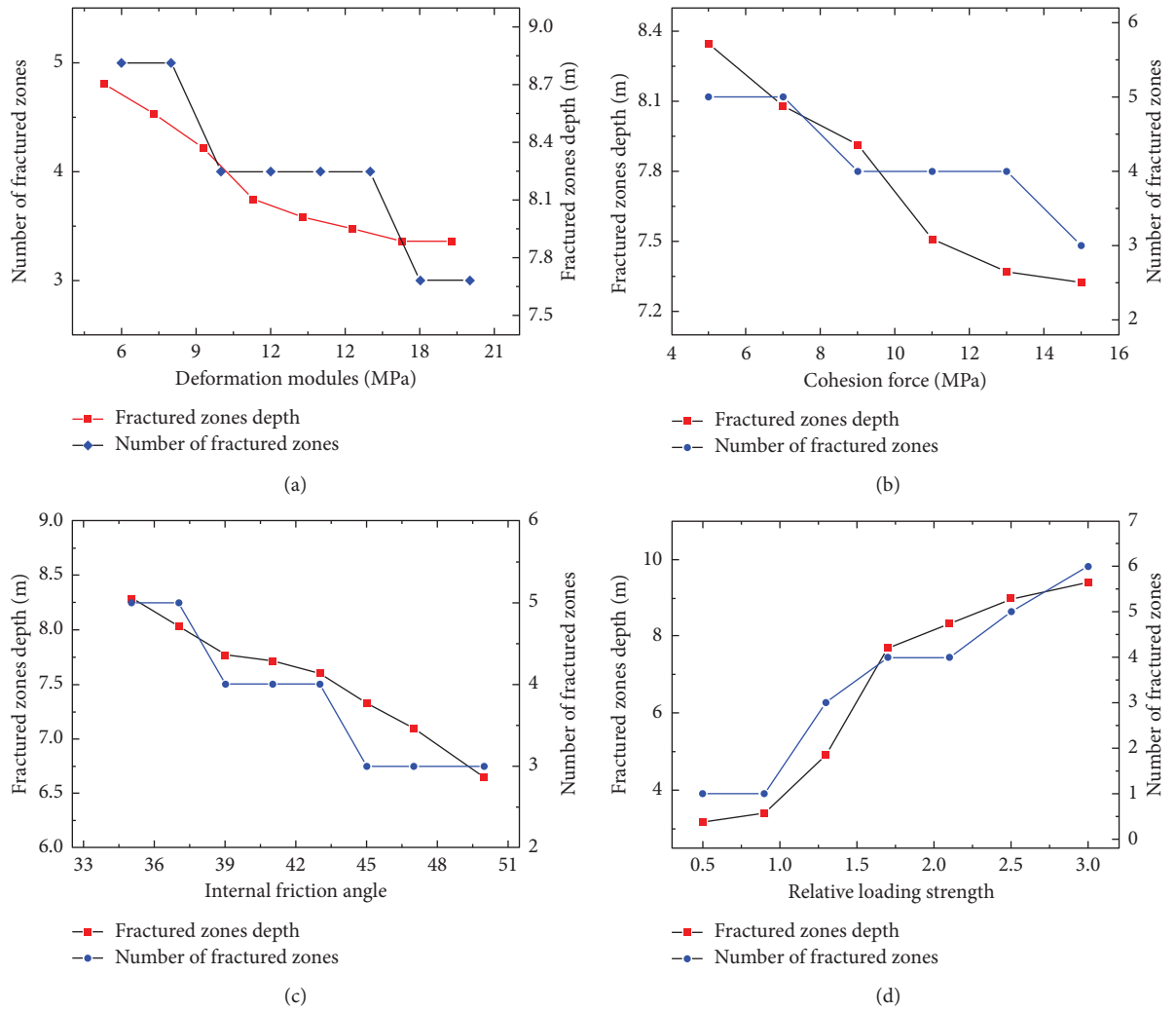

Figure 10: The statistical parameters' polyline of the various factors. (a). Deformation modulus. (b). Cohesion force. (c). Internal friction angle. (d). Relative loading strength.

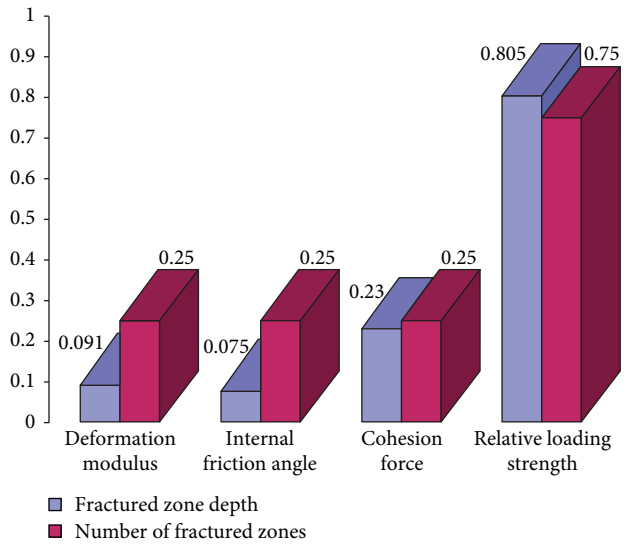

Figure 11: Histogram of sensitivity analysis.

direction of effort to improve the calculation accuracy of the calculated model through the parameter sensitivity analysis and provides a basis for the prediction and support control of different zonal disintegration modes.

Data Availability

The data used to support the findings of this study are included within the article.

Conflicts of Interest

The authors declare that there are no conflicts of interest regarding the publication of this paper.

Acknowledgments

This work was supported by the plan of science and technology of Shandong Province Colleges (grant no. J17KB046).

References

[1] E. I. Shemyakin, G. L. Fisenko, M. V. Kurlenya et al., "Zonal disintegration of rocks around underground workings, part 1: data of in situ observations," *Soviet Mining Science*, vol. 22, no. 3, pp. 157–168, 1986.

[2] H. W. Zhou, H. P. Xie, and J. P. Zuo, "Developments in researches on mechanical behaviors of rocks under the condition of high ground pressure in the depths," *Advances in Mechanics*, vol. 35, no. 1, pp. 91–99, 2005.

[3] Q. H. Qian and S. C. Li, "Review of research on zonal disintegration phenomenon in deep rock mass engineering," *Chinese Journal of Rock Mechanics & Engineering*, vol. 27, no. 6, pp. 1278–1284, 2008.

[4] J. C. Gu, L. Y. Gu, and A. M. Chen, "Model test study on mechanism of layered fracture within surrounding rock of tunnels in deep stratum," *Chinese Journal of Rock Mechanics & Engineering*, vol. 27, no. 3, pp. 433–438, 2008.

[5] Q. Y. Zhang, X. T. Zhang, W. Xiang, and X. G. Chen, "Model test study of zonal disintegration in deep rock mass under different cavern shapes and loading conditions," *Chinese Journal of Rock Mechanics & Engineering*, vol. 32, no. 8, pp. 1564–1571, 2013.

[6] C. A. Tang and Y. B. Zhang, "Discussion on mechanism and evolution laws of fracture spacing in rock mass," *Chinese Journal of Rock Mechanics & Engineering*, vol. 27, no. 7, pp. 1362–1369, 2008.

[7] F. Q. Gao, H. P. Kang, and L. Jian, "Numerical simulation of zonal disintegration of surrounding rock mass in deep mine roadways," *Journal of China Coal Society*, vol. 35, no. 1, pp. 21–25, 2010.

[8] M. Beiki, A. Bashari, and A. Majdi, "Genetic programming approach for estimating the deformation modulus of rock mass using sensitivity analysis by neural network," *International Journal of Rock Mechanics and Mining Sciences*, vol. 47, no. 7, pp. 1091–1103, 2010.

[9] M. A. Guzev and A. A. Paroshin, "Non–Euclidean Model of the Zonal Disintegration of Rocks around an Underground Working," *Journal of Applied Mechanics and Technical Physics*, vol. 42, no. 1, pp. 131–139, 2001.

[10] C. Z. Qi, Q. H. Qian, M. Y. Wang, and J. J. Chen, "Internal variable gradient plasticity model for zonal disintegration of surrounding rocks in deep tunnels," *Chinese Journal of Rock Mechanics & Engineering*, vol. 31, no. 1, pp. 2722–2728, 2012.

[11] Q. Zhang, X. Zhang, Z. Wang, W. Xiang, and J. Xue, "Failure mechanism and numerical simulation of zonal disintegration around a deep tunnel under high stress," *International Journal of Rock Mechanics and Mining Sciences*, vol. 93, pp. 344–355, 2017.

[12] M. C. He, H. P. Xie, S. P. Peng, and Y. D. Jiang, "Study on rock mechanics in deep mining engineering," *Chinese Journal of Rock Mechanics & Engineering*, vol. 24, no. 16, pp. 2803–2813, 2005.

[13] J. Li, M. Y. Wang, N. Zhang, and P. X. Fan, "Basic problems for dynamic deformation and fracture of deep rock mass," *Engineering Sciences*, vol. 15, no. 5, pp. 71–79, 2013.

[14] J. W. Zhang, "Theoretical analysis on failure zone of surrounding rock in deep large-scale soft rock roadway," *Journal of China University of Mining and Technology*, vol. 46, no. 2, pp. 292–299, 2017.

[15] Z. Fang and J. P. Harrison, "Application of a local degradation model to the analysis of brittle fracture of laboratory scale rock specimens under triaxial conditions," *International Journal of Rock Mechanics and Mining Sciences*, vol. 39, no. 4, pp. 459–476, 2002.

[16] M. G. D. Geers, *Experimental Analysis and Computational Modelling of Damage and Fracture*, Technische Universiteit Eindhoven, Eindhoven, Netherlands, 1997.

[17] S. C. Li, H. P. Wang, and Q. H. Qian, "In-situ monitoring research on zonal disintegration of surrounding rock mass in deep mine roadways," *Chinese Journal of Rock Mechanics & Engineering*, vol. 8, no. 27, pp. 1545–1553, 2008.

[18] R. Kohlmann and S. G. Gatermann, "Analysis and presentation of cumulative antimicrobial susceptibility test data–the influence of different parameters in a routine clinical microbiology laboratory," *PLoS One*, vol. 11, no. 1, Article ID e0147965, 2016.

[19] Q. Qian, X. Zhou, and E. Xia, "Effects of the axial in situ stresses on the zonal disintegration phenomenon in the surrounding rock masses around a deep circular tunnel," *Journal of Mining Science*, vol. 48, no. 2, pp. 276–285, 2012.